J Porous Mater (2014) 21:251–262
DOI 10.1007/s10934-013-9770-7

Selective formation of aniline over nanogold incorporated cobalt loaded SBA 15 catalysts

Suraja Viswanathan · Binitha Narayanan · Zahira Yaakob · Pradeepan Periyat · Silija Padikkaparambil

Published online: 1 January 2014

Abstract Nanogold was dispersed over cobalt-loaded SBA 15 to create an effective redox catalyst. The support was identified as spinel Co_3O_4 attached to mesoporous SBA 15 based on XRD, FTIR and TEM analyses. The gold crystallites were found to be in the nanosize range (8–15 nm) by the application of the Scherrer equation to the XRD data. XPS analysis provided insight into the state of the gold nanoparticles. The selective hydrogenation of nitrobenzene over nanogold doped cobalt-loaded SBA 15 catalysts was investigated in a fixed bed down flow reactor. The selectivity for the desired product, aniline, was very high with a maximum conversion of 98.9 % of nitrobenzene. The high catalytic performance is attributed to the efficient dispersion of gold nanoparticles over the support. Performing the reaction in the flow reactor maximizes the access of the reactants to the catalysts without the aid of any solvent, which further eliminates the filtration steps required to remove the catalyst after the reaction. Conducting the reaction at 200 °C facilitates the recovery of the product (aniline), from the catalyst, as soon as it is formed.

Keywords Nitrobenzene · Selective reduction · Aniline · Nanogold catalysts

S. Viswanathan · Z. Yaakob (✉) · S. Padikkaparambil
Department of Chemical and Process Engineering, Universiti Kebangsaan Malaysia (UKM), 43600 Bangi, Selangor, Malaysia
e-mail: zahirayaakob65@gmail.com

B. Narayanan
Department of Chemistry, Sree Neelakanta Government Sanskrit College, Pattambi, Palakkad 679306, Kerala, India
e-mail: binithann@yahoo.co.in

P. Periyat
Department of Chemistry, University of Calicut, Calicut, India

1 Introduction

The elimination of environmental endocrine disruptors and hazardous organic compounds has attracted increasing interest over the past two decades, because these compounds can cause severe health problems. Many aromatic nitro compounds fall under these categories [1–3]. Thus, the elimination of these compounds by conversion into valuable products is highly desired. The catalytic hydrogenation of aromatic nitro compounds is an important process for the production of amines. As a representative aromatic nitro compound, the reduction of nitrobenzene is having high relevance. Its selective conversion to aniline is essential, since aniline is widely used for the production of methylene diphenyl diisocyanate (MDI), which is an important raw material and intermediate for the production of dyes, medicines, pesticides and rubber chemicals [4]. The catalytic hydrogenation of nitrobenzene (NB) is used in approximately 85 % of aniline production globally [5]. Both liquid and vapor phase hydrogenation methods are employed using supported metal catalysts; and the liquid phase reactions generally use organic solvents, such as alcohols, acetone, benzene, ethyl acetate or aqueous acidic solutions [6–9] as the reaction medium.

The conventional method via Fe-promoted reduction in HCl (Béchamp reaction) is undesirable due to the low selectivity of amine and the production of large quantities of toxic waste, which require costly and difficult downstream separation [10]. Liquid phase hydrogenation using conventional transition metal catalysts results in increased conversion [11, 12] but reduced selectivity [13]. Moreover, the common organic solvents used in liquid phase reactions are volatile and toxic. Considering that toxicity refers to the extent to which a material can damage an organism, the use of toxic compounds in material synthesis, especially in

drug design and similar applications, is extremely undesirable. In addition, the liquid phase reduction of nitrobenzene also results in the formation of poisonous reaction intermediates such as nitrosobenzene, *N*-phenylhydroxylamine, azoxybenzene, azobenzene and hydrazobenzene [14, 15]. Au, Pt and Pd, among other catalysts, have been successfully used in hydrogenation reactions [4]. Many attempts have been made to improve the selectivity of aniline [16–19]. The use of supported Au for the batch liquid phase nitroarene reduction has resulted in high selectivity to the amine [20].

Catalyst performance depends strongly on the synthesis [21], Au particle size/shape [22] and support characteristics [23]. Different catalytic responses have been observed for supported Au on different oxides [24–28]. Wang et al. [29] have correlated catalytic performances with critical surface properties for reaction over Au on reducible ($Ce_{0.62}Zr_{0.38}O_2$) and non-reducible (Al_2O_3) supports in the gas phase hydrogenation of *p*-chloronitrobenzene (*p*-CNB). Au/Al_2O_3 promotes the exclusive production of *p*-chloroaniline (*p*-CAN), i.e., 100 % selectivity with respect to $-NO_2$ group reduction. The application of Au to promote $-NO_2$ group hydrogenation was reported by Cardenas-Lizana et al. [30] in their study of the gas phase hydrogenation of *m*-dinitrobenzene (*m*-DNB) over Au catalysts, which yielded a time-invariant conversion (for up to 5 h) and 100 % selectivity in terms of $-NO_2$ group reduction, i.e., no evidence of hydrodenitrogenation and/or aromatic ring reduction [30]. The combined catalytic action of Au with Mo_2C for the gas phase hydrogenation of substituted nitroarenes resulted in a higher hydrogenation efficiency for the conversion of *p*-CNB and *m*-DNB, exceeding the performance of Au/Al_2O_3. The exclusive formation of the partially reduced m-nitroaniline (m-NAN) was enhanced over Au/Mo_2C relative to Mo_2C under conditions in which Au/Al_2O_3 was non-selective in the hydrogenation of m-DNB [31]. Gas phase hydrogenation of *p*-CNB to *p*-CAN over oxide (Al_2O_3, TiO_2, Fe_2O_3 and CeO_2)-supported Au has been reported to be highly selective [32–35]. The role of Au particle size in hydrogenation reactions appears to depend on the nature of the reaction [36], the support [37] and even the catalyst preparation method [38]. Although Au particles as large as 20 nm can exhibit significant activity under optimum reaction conditions [39], the general trend suggests that smaller Au particles (<10 nm) yield higher hydrogenation [28]. Catalyst deactivation in the gas phase hydrogenation of nitroarenes over Pd/Al_2O_3 [40–42], Pd/hydrotalcite [5], Cu/SiO_2 [43] and Cu/Kieselguhr [44] has been reported and ascribed to the deleterious effect of H_2O as a by-product [5], metal leaching [42] and coking [40, 41, 43, 44]. Not only the particle size but also the nature of the support plays an important role in catalysis [45–48]. The role of the support may exceed that of a stabilizer of the Au dispersion or a modifier of the Au electronic state. When gold is dispersed on supports with a high surface area, its catalytic properties change substantially. For supported gold catalysts, the agglomeration of gold particles is a major cause of catalyst deactivation. The porosity of the support plays an important role in facilitating metal particle agglomeration [49, 50].

The main drawback associated with nitrobenzene reduction via vapor or liquid phase hydrogenation is the severe reaction conditions required, i.e., higher reaction temperature or pressure respectively. Therefore, it is of greater interest to improve the catalytic activity under mild reaction conditions. Supported noble metals (Pt, Pd, etc.) or Raney Ni are the most commonly employed hydrogenation catalysts of nitrobenzene [4]. In most cases, high conversion is attained, but 100 % selectivity to the amino compound has not been commonly achieved [34].

In the present study, gold nanoparticles are immobilized over cobalt-loaded SBA 15 support, where the porosity of the support can contribute shape selectivity to the products. As a representative hazardous aromatic nitro compound, the selective reduction of nitrobenzene to aniline, an important product, is investigated here. The nitrobenzene reduction is conducted in a vertical down-flow fixed-bed reactor over nanogold-incorporated cobalt-loaded SBA 15 catalysts. The catalysts have been characterized to identify the catalyst with the best performance and the optimal reaction conditions. The percentage gold loading is also varied to achieve maximum conversion. The high conversion acquired under mild conditions with Co/SBA 15 supported Au catalysts indicates that the cobalt doped SBA 15 materials are promising support materials for nanogold dispersion.

2 Experimental

2.1 Preparation of SBA-15

The support, SBA 15 was prepared using a previously reported method [51]. The preparation required 4.4 g of Pluronic P123 (Aldrich, $M_{average} = 5{,}800$ [EO20-PO70-EO20]), 120 g of 2 M HCl (R&M Chemicals) and 9 g of TEOS (Aldrich). The triblock copolymer P123 was dispersed in 30 g of distilled water and stirred for 1.5 h. 2 M HCl was added to the resultant solution under stirring, which was continued for 2 h. Finally, TEOS was added dropwise, and the mixture was maintained at room temperature for 24 h with stirring. The resultant heterogeneous mixture was subjected to hydrothermal treatment at 100 °C for 48 h under static conditions before recovering the solid material. The crystallized product was filtered, washed with distilled water and dried in air for 24 h and in an oven at 70 °C overnight before being calcined at 450 °C for 8 h to remove the template completely.

2.2 Preparation of cobalt-loaded SBA 15

Cobalt loading was performed on SBA 15 by a simple impregnation method. Cobalt nitrate hexahydrate (Hamburg Chemical GmbH) was dissolved in water. A predetermined amount of prepared SBA 15 was then added to this solution, followed by heating at 80 °C under stirring to remove the solvent. The amount of cobalt nitrate was varied to obtain samples with different wt% (10–50 %) of cobalt/g SBA 15. The concentrated sample was dried in oven at 80 °C overnight. The dried sample was then calcined at 400 °C for 5 h and designated as *x*Co/SBA 15, where *x* indicates the % cobalt loading.

2.3 Preparation of Au doped Co/SBA 15

Aqueous chloroauric acid (2.1×10^{-3} M; Sigma Aldrich) solution was heated to 70 °C. The pH of the solution was adjusted to 8 by the drop wise addition of 0.5 M NaOH (R & M Chemicals). The required amount of Co/SBA 15 was added to the above mixture at constant pH and temperature (8 and 70 °C respectively) under vigorous stirring. The mixture was maintained under the above conditions with stirring for an additional 2 h and then cooled, filtered and washed with distilled water. The mixture was then dried at 80 °C overnight and calcined at 200 °C for 5 h. The systems were designated as nAu-xCo/SBA 15, where n and x indicate weight percentage of gold and cobalt respectively.

2.4 Preparation of Co_3O_4 and Au doped Co_3O_4

For catalytic activity comparison, bulk Co_3O_4 and its Au doped counterpart were also prepared using the conventional precipitation method. First, 0.5 mol/L cobalt nitrate hexahydrate solution was precipitated by ammonia. The pH was maintained between 7.5 and 8.5, and the solution was stirred for 4 h. The resulting precipitate was aged at room temperature for 24 h before being filtered and washed with water. The precipitate was dried at 80 °C overnight and calcined at 400 °C for 5 h. Finally, 1 wt% Au was then loaded using the method described in Sect. 2.3. The systems were designated as Co_3O_4ppt and 1Au–Co_3O_4ppt.

2.5 Catalyst characterization

The XRD patterns of the samples were recorded in the range of $2\theta = 3$–80° on a Bruker AXS D8 Advance diffractometer at a scanning rate of 0.02°/s with Cu Kα radiation ($\lambda = 1.5418$). The FTIR spectra were recorded using a Thermo Scientific Nicolet 6700 FT-IR spectrometer in the wavelength range of 400–4,000 cm^{-1}. The formation of well-ordered mesopores of SBA 15 was confirmed using TEM (Zeiss Libra 200). X-ray photoelectron spectroscopy (XPS) was conducted using a Kratos XSAM X-ray photoelectron spectrometer with a base pressure of 10^{-9} Torr. Mg Kα X-ray radiation was used as the excitation source. The binding energy of C 1s (284.5 eV) was used as the reference to correct any charge offsets. Linear background subtraction was performed, and the peaks in each spectrum were fitted using a Gaussian function. The BET surface area and pore volume were measured using a TriStar 3000 V6.04 A instrument, using nitrogen physisorption at −195.800 °C. The specific surface area was estimated using the BET method. The pore size distribution and pore volume were determined by the BJH method. All systems were activated at the calcination temperature for 1 h before characterization. Elemental analysis of 1Au-40Co/SBA 15 was done using Inductively Coupled Plasma Atomic Emission Spectrometer (ICP—AES, Thermo Electron IRIS INTREPID II XSP DUO).

2.6 Catalytic activity: hydrogenation of nitrobenzene

The catalytic hydrogenation of NB without the aid of any solvent under H_2 flow was carried out at atmospheric pressure in a down-flow vertical fixed bed glass reactor (length = 41 cm, i.d. = 1.4 cm) placed inside a double-zone furnace. The reaction was performed to ensure negligible heat/mass transport limitations, as described elsewhere [52–54], with some specified features pertinent to this study. The catalysts were activated at the calcinations temperature for 1 h before being subjected to catalytic activity studies. The temperature was continuously monitored by a thermocouple. The NB was fed into the reactor via an airtight glass syringe and Teflon line using a microprocessor-controlled syringe pump (New Era Pump Systems Inc. E905120) at a fixed and calibrated flow rate. The product and the unreacted NB were trapped and condensed by a water condenser. The liquid samples were then analyzed using a gas chromatograph (SRI 8610 gas chromatograph) equipped with a RESTEK RXi-1 ms column and an FID detector using N_2 as the carrier gas. The catalyst activity is presented in terms of the percentage of NB converted.

3 Results and discussion

3.1 Material characterization

The wide-angle XRD patterns for different samples are shown in Fig. 1. All catalyst systems exhibit a major peak characteristic of spinel Co_3O_4 at $2\theta = 36.8°$. The diffraction peaks at $2\theta = 19.0°$, 31.3°, 36.8°, 44.80°, 59.2° and 65.1° can also be attributed to the spinel type cubic structure of Co_3O_4 with an Fd3m space group [55]. The peak becomes more intense and narrow as the percentage loading of Co on SBA 15 increases, indicating the gradual growth of the

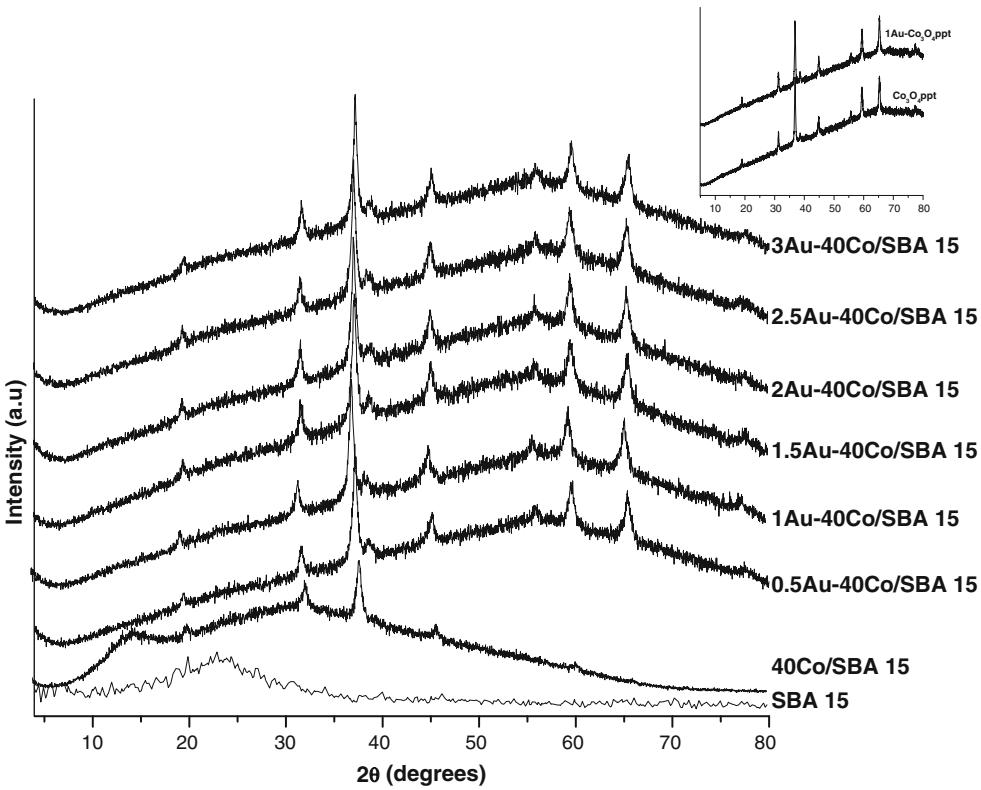

Fig. 1 XRD patterns of the prepared systems

Co_3O_4 crystallites. Based on the Scherrer equation, the crystallite size of Co_3O_4 in 40Co/SBA 15 is found to be 14.8 nm. The diffraction peaks for metallic gold appear at approximately 38.3°, 45° and 64.5° respectively, corresponding to the (111), (200) and (220) lattice planes of the face-centered cubic structure of gold, respectively [56]. Due to the support interference and small particle sizes, the Au peaks at 45° and 64.5° are not clearly visible. The Au crystallite size is calculated from the peak at approximately 38.3°. From the data shown in Table 1, it can be noted that all of the samples contained gold nanocrystallites ranging in size from 8 to 15 nm.

The FT-IR spectra of the calcined SBA-15, *n*Co/SBA-15, Au–Co/SBA 15 and Co_3O_4ppt between 400 and 4,000 cm^{-1} are presented in Fig. 2. In the spectrum of raw SBA 15, the three peaks at 470, 799 and 1,090 cm^{-1} correspond to the rocking, bending (or symmetric stretching) and asymmetric stretching modes, respectively, of the inter tetrahedral oxygen atoms in the SiO_2 structure [57, 58]. The broad band from 3,400 to 3,700 cm^{-1} is assigned to the stretching frequencies of hydrogen-bound silanols as well as adsorbed H_2O. The absorption bands of spinel Co_3O_4 at approximately 667 and 565 cm^{-1} are clearly observed in the spectra of the 40Co/SBA 15 samples [59]. As it can be observed, the IR peaks related to the stretching vibrations of the functional groups of the SBA 15 are present in the spectra of Co/SBA 15 and nAu–Co/SBA 15, indicating that

Table 1 Au crystallite size and NB reduction data over different catalysts under the selected conditions

Catalyst	NB conversion (%)	Aniline selectivity (%)	Au crystallite size (nm)
No catalyst	–	–	–
SBA 15	–	–	–
40Co/SBA 15	66.27	94.98	–
0.5Au–40Co/SBA 15	83.14	94.85	10.75
1Au–40Co/SBA 15	96.88	100	9.75
1.5Au–40Co/SBA 15	89.06	98.75	14.75
2Au–40Co/SBA 15	92.65	98.46	8.23
2.5Au–40Co/SBA 15	94.65	94.94	9.75
3Au–40Co/SBA 15	98.85	100	12.13
Coppt	17.27	94.92	–
1AuCoppt	47.17	95.98	19.31

Reaction conditions: catalyst weight = 0.2 g, temperature = 200 °C, flow rate = 4 ml/h

no structural deformation of the basic structure of SBA 15 occurred upon metal doping. Figure 3 shows the TEM images of some representative systems. The grey region represents for silica walls and the dark regions contain spinel cobalt, on which the gold nanoparticles may be distributed. The Au particles on the top of Co_3O_4 were visible whenever the Co species where present towards the edges of SBA 15 support.

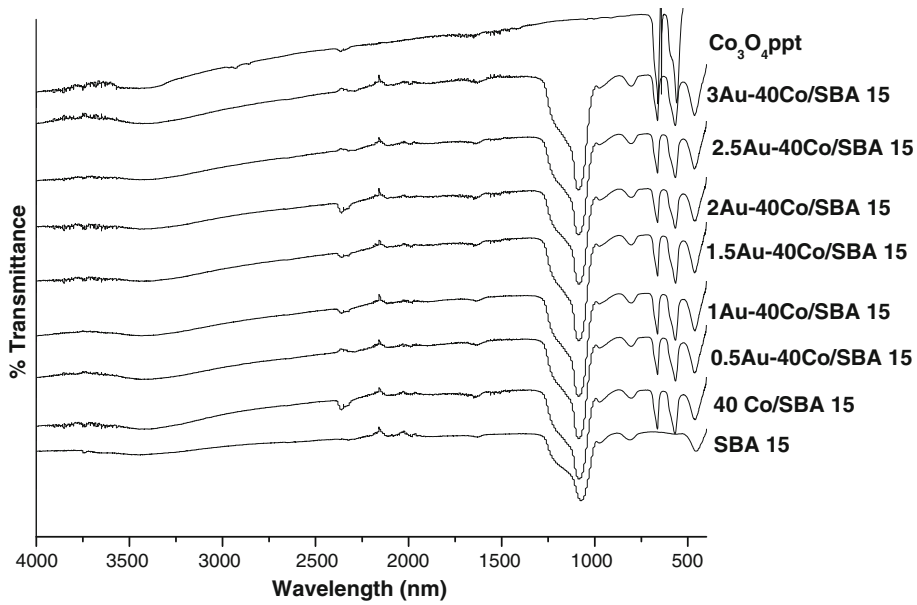

Fig. 2 FTIR spectra of the different catalysts

A comparative XPS study of bare 40Co/SBA 15 and gold-doped 40Co/SBA 15 has been carried out. The XPS spectra showed signs of the presence of cobalt, silicon, oxygen, carbon and gold in the gold-loaded sample. The carbon peak is the result of hydrocarbon layer contamination and is unavoidable in the XPS analysis [60]. In-depth XPS analyses of the $Au4f_{7/2}$, $Co2p_{3/2}$, Si2p and O1s regions were conducted to identify the chemical composition and oxidation state. Spectral deconvolution was achieved using a Gaussian-fitting procedure (Fig. 4a–c).

The XPS signals for cobalt arise from the $2p_{3/2}$ and $2p_{1/2}$ levels. The coexistence of Co^{2+}/Co^{3+} resulted in a main peak at BE = 779.9 eV, supporting the existence of the spinel phase of Co_3O_4 [61]. This observation supports the existence of Co_3O_4 as the predominant cobalt phase in the catalyst, as evident from the XRD and FTIR analyses. Sexton et al. [62] reported a binding energy of 780.3 eV for Co^{2+} and 779.5 eV for Co^{3+}. The two peaks centered at binding energies of 530.1 ± 0.1 and 532.5 ± 0.2 eV correspond to the Co–O bond in the spinel and the Si–O bond in SiO_2 respectively [60]. The peak at 529.6 eV is due to the lattice oxygen of cobalt oxides [63]. The BE at 103.5 eV is due to SiO_2. The Au 4f patterns are characteristic of the predominant metallic gold [64]. Large particles and/or composite islands of metallic gold account for the existence of a peak at 83.6 eV [65]. However, in the case of the present 1Au–40Co/SBA 15 system, this band is shifted to a higher BE of 84.6 eV and is associated with smaller Au^0 particles [65]. The peak at 85.1 ± 0.1 eV can be tentatively assigned to Au^{+1} species [66–68]. In the literature, zero-valent [69] and cationic Au [70] have been proposed to promote hydrogenation. In the present study, we also attribute this phenomenon to the presence of nanogold in the catalysts.

The adsorption-desorption isotherms for SBA-15, 40Co/SBA-15 and some selected Au-loaded 40Co/SBA 15 samples are presented in Fig. 5a. All samples displayed type IV isotherms, which are attributed to typical mesoporous structures. Hysteresis loops, which are present in conventional mesoporous silicas, were also found in the present catalysts. SBA 15 exhibits a low-pressure hysteresis that extends to the lowest attainable pressures, indicating the presence of micropores. The narrow pore size distribution depicted in Fig. 5b confirms the regularity of the pore diameter. The similarity in the adsorption-desorption curves and hysteresis loops indicates that all of the samples have similar pores.

The specific area, average pore volume and average pore diameter of pure SBA-15, 40Co/SBA-15 and Au-loaded Co/SBA 15 catalysts are listed in Table 2. Metal doping resulted in the blockage of the support pores by cobalt oxide, reducing the BET surface area and pore volume [71] by making the pores inaccessible for nitrogen adsorption. The leaching of Si from the matrix may be the cause of the increase in the average pore diameter. After the deposition of gold nanoparticles on cobalt-containing SBA-15, a considerable expansion in the pore-size and a noticeable decrease in the surface area were observed in addition to a decrease in pore volume, which may result from the partial degradation of the silica matrix [72].

3.2 Catalytic behavior

The hydrogenation of nitrobenzene over the Au–Co/SBA 15 catalysts resulted in the formation of aniline with very high selectivity. No hydrogenation was observed without the catalyst, indicating the absence of any uncatalyzed

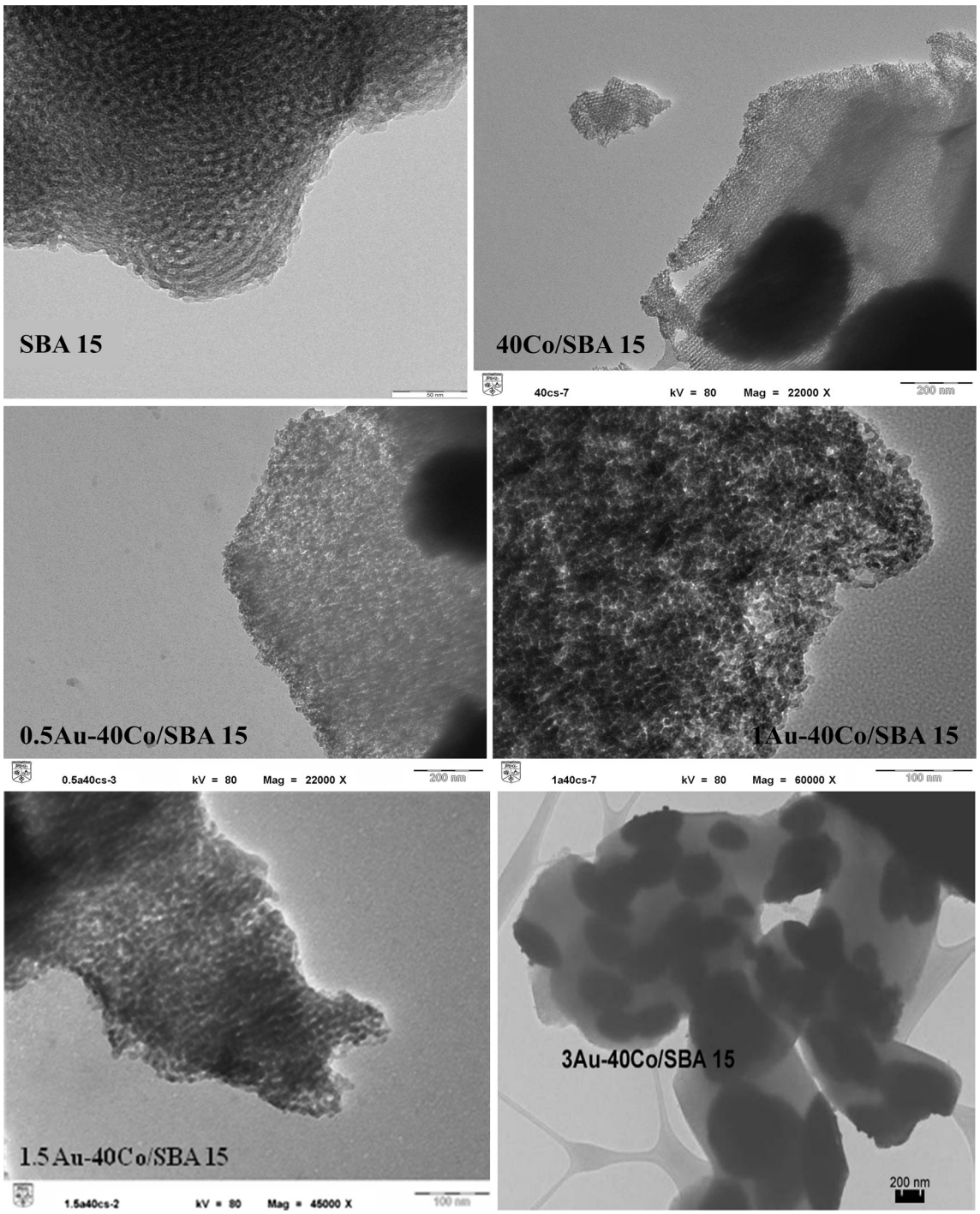

Fig. 3 TEM images showing the dispersion of cobalt oxide and nanogold particles over the SBA 15 support

reaction. No conversion was found over pure SBA 15, which suggests that SBA 15 acts as an inactive support. The effect of the reaction variables, including temperature, catalyst amount and NB flow rate, as well as the effect of the extent of nanogold incorporation on Co/SBA 15 was thoroughly investigated. Preliminary tests were carried out using 2 wt% Au-doped Co-loaded SBA 15 catalysts with various Co loadings to study the influence of the percentage of Co loading over SBA 15 on its catalytic activity. The results, which are given in Table 3 reveal that 40 wt% Co over SBA 15 is the best support for nitrobenzene hydrogenation reactions. Therefore, further studies were performed with gold-doped 40Co/SBA 15 catalysts. All catalysts promoted the exclusive $-NO_2$ group hydrogenation with no evidence of hydrodenitrogenation and/or aromatic ring reduction. The effect of the reaction

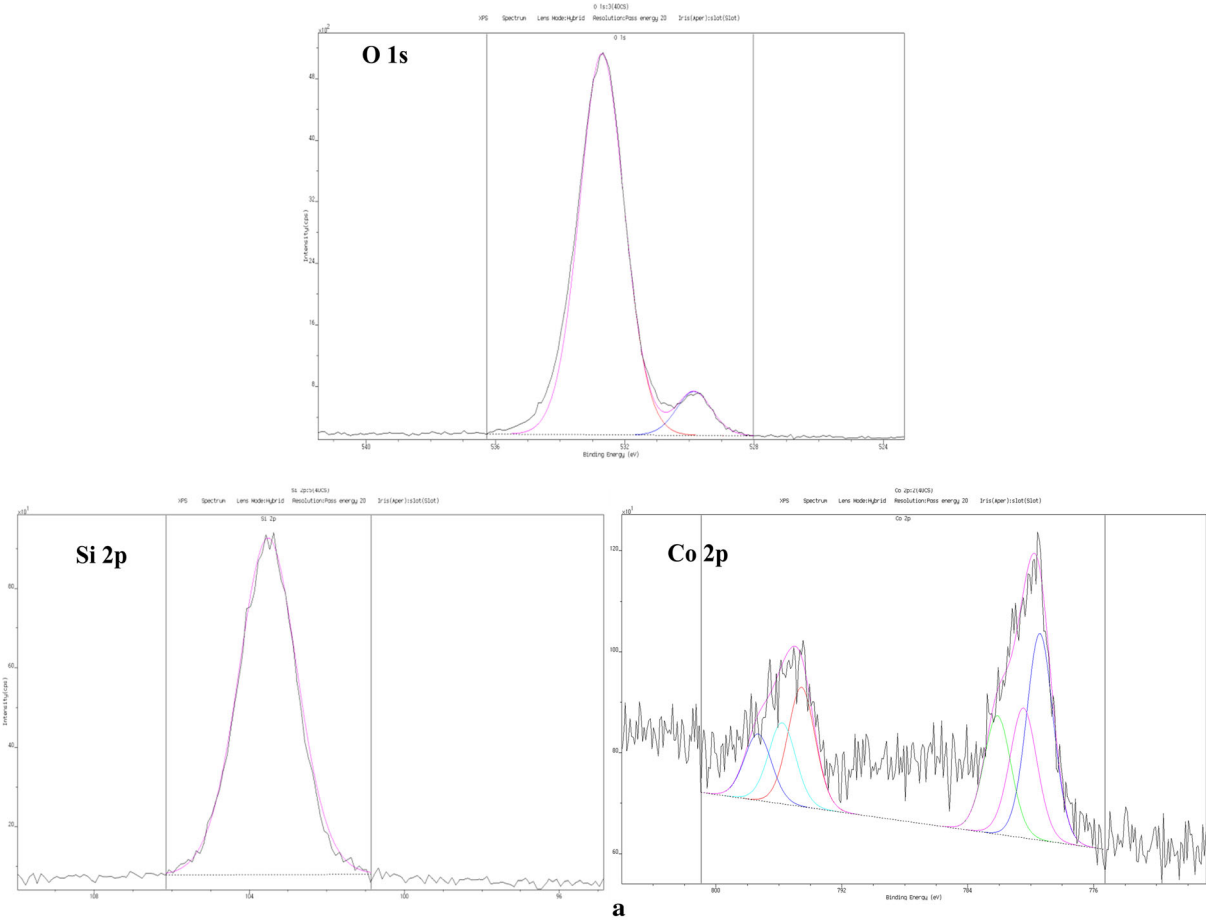
O 1s
Si 2p
Co 2p
a
O 1s
Co 2p
Si 2p
Au 4f
b

◀**Fig. 4** **a** The de-convolution XPS analysis of the O 1s, Si 2p and Co 2p core-level peaks for 40Co/SBA 15. **b** The de-convolution XPS analysis of the O 1s, Si 2p, Co 2p and Au 4f core-level peaks for 1Au–40Co/SBA 15. **c** XPS wide-angle spectra of 40Co/SBA 15 and 1Au–40Co/SBA 15

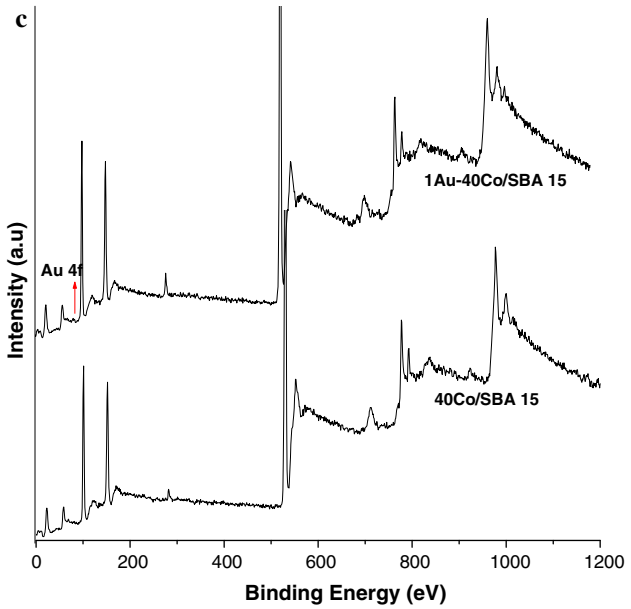

Fig. 4 continued

parameters was investigated over 1Au–40Co/SBA 15. In order to investigate the turn over number (TON) of the reaction (moles aniline/moles Au) under various conditions, elemental analysis of 1Au–40CoSBA 15 is carried out and it is found that the amount of Au present is 7.3365×10^{-6} mol/g of the catalyst.

3.2.1 *Effect of temperature*

Temperature had a marked effect on activity. Figure 6 shows the influence of temperature on the hydrogenation of nitrobenzene over the 1Au–40Co/SBA 15 catalyst. First, the temperature was varied in the range of 200–400 °C in 50 °C intervals. As the temperature increased, the rate of nitrobenzene conversion decreased. Therefore, we also tested the activity under the low temperatures of 195 and 190 °C. The activity decreased at these temperatures; thus, we selected 200 °C for further studies. Here, the best reaction temperature is lower than the boiling point of nitrobenzene. However, at this temperature, the product aniline is vaporized and diffuses out of the catalyst as soon as it is formed, freeing the active sites for further catalysis. This phenomenon may be the cause of the improved activity. Further increases in temperature yield reductions in activity, which might be due to the low contact time as a result of the ready diffusion of some of the reactants in the out of the catalyst before successful reaction.

3.2.2 *Effect of catalyst weight*

The NB conversion initially increased with increasing catalyst dosage, with the selectivity remaining at 100 %, except at a high catalyst dosage of 0.25 g. The highest conversion was obtained using 0.2 g of catalyst, beyond which the conversion rate decreased (Fig. 7). Higher amounts of the catalyst provided more active sites for effective catalysis; however, this effect was saturated at a catalyst loading of 0.2 g. Further increases in the catalyst weight decreased the activity, possibly due to the restricted movement of the reaction mixture out of the catalyst surface. From the figure, it can be seen that use of 0.1 g catalyst resulted in the highest turnover number for the reaction. Based on the number of moles of Au required for the effective formation of aniline, 0.1 g catalyst was found to be the most desired catalyst dosage for the reaction.

3.2.3 *Influence of flow rate*

The catalysts/reactant flow rate was varied from 3 mL/h to study its influence on NB conversion, TON and aniline selectivity (Fig. 8). The selectivity remained at 100 % in all cases studied, whereas the conversion decreased beyond a flow rate of 4 mL/h. The decrease in conversion at higher flow rates may be due to the reduced contact time [73]. We had also calculated the moles of aniline formed over moles of Au (TON); and it was observed that 4 mL/h is the best flow rate for the effective reaction. Thus, we selected a flow rate of 4 mL/h for further study.

3.2.4 *Comparison of catalytic efficiency over Au-doped systems*

NB reduction was carried out over 40 %-Co-loaded SBA 15 systems with varying amounts of doped nanogold under the following selected reaction conditions: catalyst weight, 0.2 g; NB flow rate 4 mL/h; reaction temperature, 200 °C. All gold-doped samples showed good conversion of NB, as shown in Table 1. The successful adsorption of the reactants over the catalyst surface, porous nature of the support, easy diffusion of the product etc. may be the reason for the high selectivity towards aniline. The high activity may also be attributed to the low particle size of nanogold, as well as the "zero" oxidation state of the nanosized gold particles and the presence of cationic Au as evident from XPS analysis. The activity initially increased with the percentage of Au, followed by slight decrease in NB conversion and then an increase to give a maximum conversion of 98.9 % over 3Au–40Co/SBA 15. To determine whether the

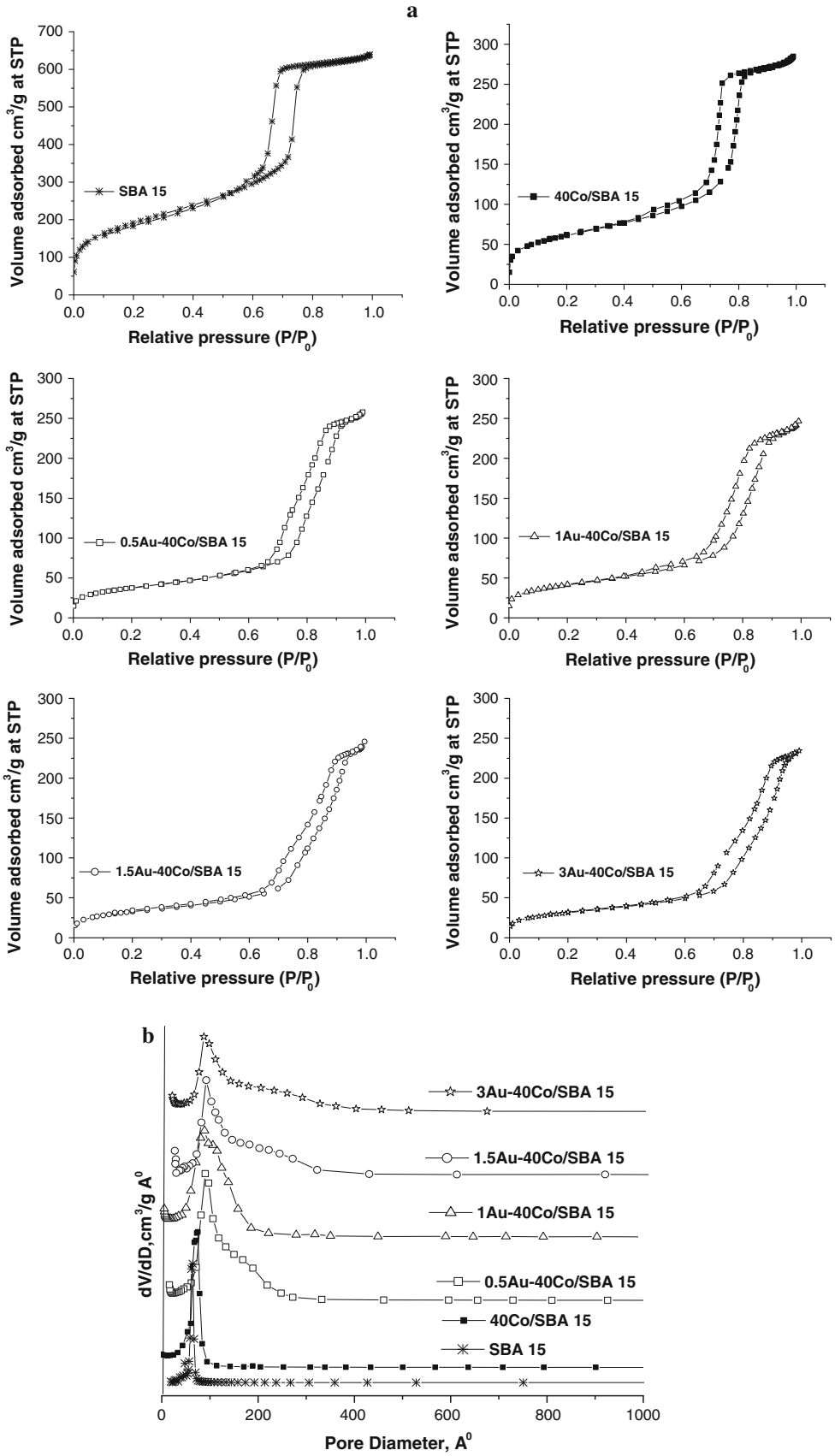

Fig. 5 **a** Nitrogen adsorption/desorption isotherms. **b** Pore size distributions of different samples

Table 2 Textural properties of the supports and catalysts

System	BET surface area (m^2/g)	Pore volume (cm^3/g)	Pore diameter (Å)
SBA 15	683.99	0.9600	60.87
40Co/SBA 15	213.62	0.4476	70.37
0.5Au–40Co/SBA 15	131.32	0.4015	92.40
1Au–40Co/SBA 15	144.30	0.3848	84.95
1.5Au–40Co/SBA 15	113.95	0.3824	101.27
3Au–40Co/SBA 15	109.49	0.3648	99.49

Table 3 Preliminary studies to obtain the best Co wt% on SBA 15 support for gold doping for NB reduction

Catalyst weight = 0.2 g, temperature = 200 °C, flow rate = 4 mL/h

Catalyst	Conversion	Selectivity
No catalyst	0	0
SBA 15	0	0
2Au–10Co/SBA 15	65.27	98.21
2Au–20Co/SBA 15	60.32	97.76
2Au–30Co/SBA 15	80.41	96.32
2Au–40Co/SBA 15	92.65	98.46
2Au–50Co/SBA 15	80.77	98.44

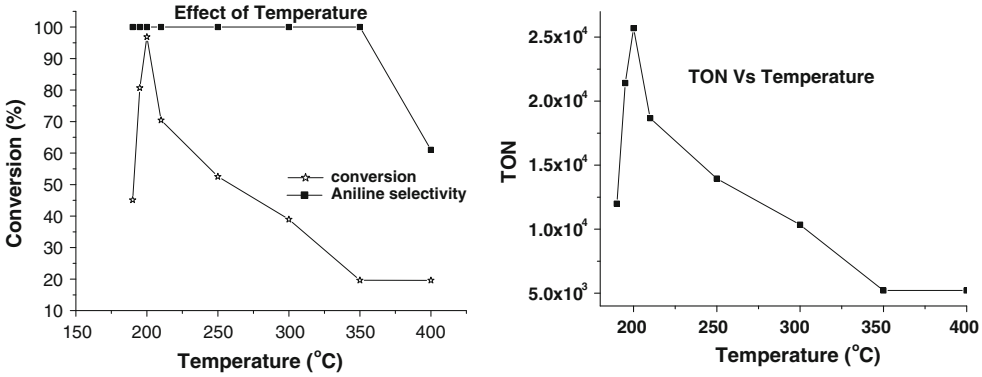

Fig. 6 Effect of temperature on NB reduction at a catalyst dosage of 0.20 g and a flow rate of 4 ml/h

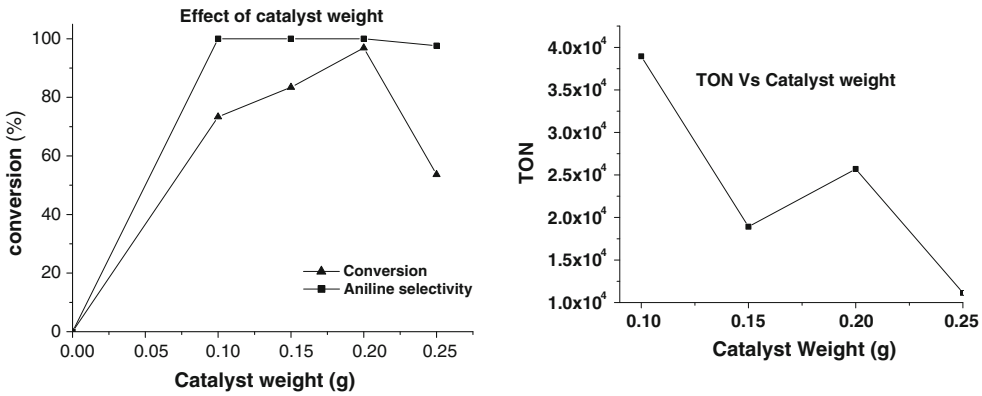

Fig. 7 Effect of catalyst weight on NB reduction at 200 °C and at a flow rate of 4 ml/h

support, Co/SBA 15, plays an important role in the catalytic activity, the reaction was also conducted over bare spinel Co_3O_4 and its gold-doped counterpart, 1Au–Co_3O_4ppt (XRD patterns confirmed the spinel structure (Fig. 1). The activity was poor, and the gold-doped system provided an even lower conversion than the active support in the present study, i.e., 40Co/SBA 15. This confirms the efficiency of the present catalyst supports for the effective

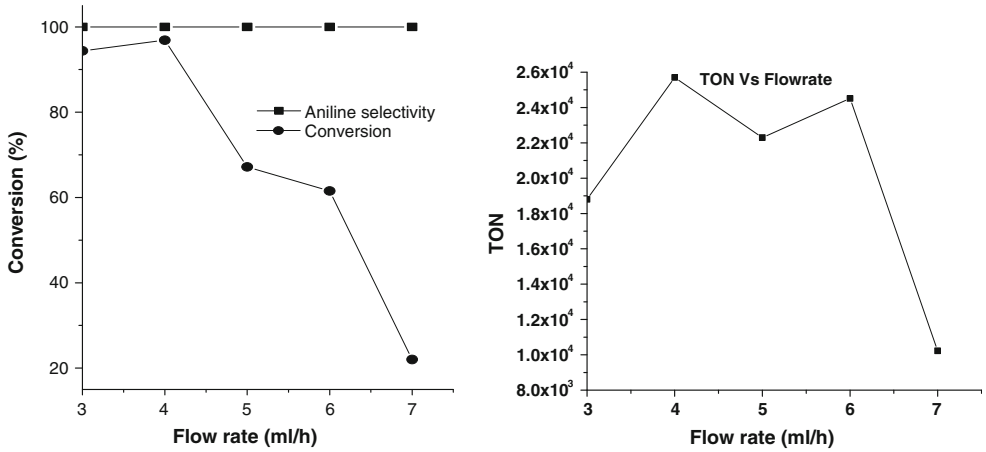

Fig. 8 Effect of flow rate on NB reduction over a catalyst dosage of 0.20 g at 200 °C

dispersion of nanogold, making it as a highly promising catalyst for NB reduction.

4 Conclusions

The selective hydrogenation of NB to aniline over nanogold-doped cobalt-loaded mesoporous SBA 15 catalysts was investigated in a fixed bed down flow reactor. The selectivity for the desired product is 100 % with 98.9 % conversion over the best catalyst, 3Au–40Co/SBA 15, under the selected reaction conditions. Even the 1 %-gold-loaded sample yielded 96.9 % conversion at a low reaction temperature of 200 °C. The high catalytic performance of the present catalysts is attributed to the efficient dispersion of gold nanoparticles, as evident from XRD and TEM analysis. XPS analysis revealed the presence of zero-valent and cationic Au, which promote the hydrogenation reaction over the prepared systems.

Acknowledgments The authors acknowledge financial assistance in the form of UKM Grant-UKM-RF-06-FRGS0106-2010. Binitha Narayanan thanks University Grants Commission, New Delhi, India, for UGC Research Award.

References

1. G.C. Muller, U.H. Kim, Endocrinology **102**, 1429–1435 (1978)
2. R. White, S. Jobling, S.A. Hoare, J.P. Sumpter, M.G. Parker, Endocrinology **135**, 175–182 (1994)
3. C. Furuta, A.K. Suzuki, S. Taneda, K. Kamata, H. Hayashi, Y. Mori, C. Li, G. Watanabe, K. Taya, Biol. Reprod. **70**, 1527–1533 (2004)
4. N. Mahata, A.F. Cunha, J.J.M. Órfao, J.L. Figueiredo, Appl. Catal. A: Gen. **351**, 204–209 (2008)
5. P. Sangeetha, P. Seetharamulu, K. Shanthi, S. Narayanan, K.S. Rama Rao, J. Mol. Catal. A: Chem. **273**, 244–249 (2007)
6. E.A. Gelder, S.D. Jackson, C.M. Lok, Catal. Lett. **84**, 205–206 (2002)
7. F. Figueras, B. Coq, J. Mol. Catal. A: Chem. **173**, 223 (2001)
8. C.C. Torres, E.L. Jablonski, G.T. Baronetti, A.A. Castro, S.R. de Miguel, O.A. Scelza, M.D. Blanco, M.A. Pena Jimenez, L.G. Fierro, Appl. Catal. A **161**, 213 (1997)
9. M.C. Macias Perez, C. Salinas Martinez de Lecea, A. Linares Solano, Appl. Catal. A **151**, 461–475 (1997)
10. X.D. Wang, M.H. Liang, J.L. Zhang, Y. Wang, Curr. Org. Chem. **11**, 299–314 (2007)
11. X. Yan, J. Sun, Y. Wang, J. Yang, J. Mol. Catal. A: Chem. **252**, 17–22 (2006)
12. H. Liu, J. Deng, W. Li, Catal. Lett. **137**, 261–266 (2010)
13. H.U. Blaser, H. Steiner, M. Studer, Chem. Cat. Chem. **1**, 210–221 (2009)
14. F.C. Lizana, S.G. Quero, M.A. Keane, Appl. Catal. A **334**, 199–206 (2008)
15. E. Baumgarten, A. Fiebes, A. Stumpe, React. Funct. Polym. **33**, 71–79 (1997)
16. H. Li, Q. Zhao, H. Li, J. Mol. Catal. A: Chem. **285**, 29–35 (2008)
17. N. Yao, J. Chen, J. Zhang, J. Zhang, Catal. Commun. **9**, 1510–1516 (2008)
18. X.X. Han, Q. Chen, R.X. Zhou, J. Mol. Catal. A: Chem. **277**, 210–214 (2007)
19. X. Yang, H. Liu, H. Zhong, J. Mol. Catal. A: Chem. **147**, 55–62 (1999)
20. A. Corma, P. Sema, P. Concepcion, J.J. Calvino, J. Am. Chem. Soc. **130**, 8748–8753 (2008)
21. G.C. Bond, D.T. Thompson, Catal. Rev. **41**, 319–388 (1999)
22. C. Mohr, H. Hofmeister, P. Claus, J. Catal. **213**, 86–94 (2003)
23. C. Milone, C. Crisafulli, R. Ingoglia, L. Schipilliti, S. Galvagno, Catal. Today **122**, 341–351 (2007)
24. X. Zhang, A. Corma, Angew. Chem. Int. Ed. **47**, 4358–4361 (2008)
25. M. Boronat, P. Concepcion, A. Corma, S. Gonzalez, F. Illas, P. Serna, J. Am. Chem. Soc. **129**, 16230–16237 (2007)
26. L.F. Liotta, Catalysts **2**, 299–302 (2012)
27. M. Shekhar, J. Wang, W.S. Lee, W.D. Williams, S.M. Kim, E.A. Stach, J.T. Miller, W.N. Delgass, F.H. Ribeiro, J. Am. Chem. Soc. **134**, 4700–4708 (2012)
28. P. Claus, Appl. Catal. A **291**, 222–229 (2005)
29. X. Wang, N. Perret, J.J. Delgado, G. Blanco, X. Chen, C.M. Olmos, S. Bernal, M.A. Keane, J. Phys. Chem. C **117**, 994–1005 (2013)
30. F. Cárdenas-Lizana, S. Gómez-Quero, N. Perret, M.A. Keane, Catal. Sci. Technol. **1**, 652–661 (2011)
31. N. Perret, X. Wang, L. Delannoy, C. Potvin, C. Louis, M.A. Keane, J. Catal. **286**, 172–183 (2012)

32. F. Cardenas-Lizana, S. Gomez-Quero, N. Perret, M.A. Keane, Gold Bull. **42**, 124–132 (2009)
33. F. Cardenas-Lizana, S. Gomez-Quero, A. Hugon, L. Delannoy, C. Louis, M.A. Keane, J. Catal. **262**, 235–243 (2009)
34. F. Cardenas-Lizana, S. Gomez-Quero, M.A. Keane, Catal. Commun. **9**, 475–481 (2008)
35. F. Cardenas-Lizana, S. Gomez-Quero, M.A. Keane, Chem. Sus. Chem. **1**, 215–221 (2008)
36. H. Sakurai, M. Haruta, Appl. Catal. A **127**, 93–105 (1995)
37. C. Milone, R. Ingoglia, L. Schipilliti, C. Crisafulli, G. Neri, S. Galvagno, J. Catal. **236**, 80–90 (2005)
38. S. Schimpf, M. Lucas, C. Mohr, U. Rodemerck, A. Bruckner, J. Radnick, H. Hofmeister, P. Claus, Catal. Today **72**, 63–78 (2002)
39. J.E. Bailie, H.A. Abdullah, J.A. Anderson, C.H. Rochester, N.V. Richardson, N. Hodge, J.G. Zhang, A. Burrows, C.J. Kiely, G.J. Hutchings, Phys. Chem. Chem. Phys. **3**, 4113–4121 (2001)
40. E. Klemm, B. Amon, H. Redlingshofer, E. Dieterich, G. Emig, Chem. Eng. Sci. **56**, 1347–1353 (2001)
41. V. Vishwanathan, V. Jayasri, P.M. Basha, N. Mahata, L.M. Sikhwivhilu, N.J. Coville, Catal. Commun. **9**, 453–458 (2008)
42. K.K. Yeong, A. Gavriilidis, R. Zapf, V. Hessel, Catal. Today **81**, 641–651 (2003)
43. S. Diao, W. Qian, G. Luo, F. Wei, Y. Wang, Appl. Catal. A **286**, 30–35 (2005)
44. L. Petrov, K. Kumbilieva, N. Kirkov, Appl. Catal. **59**, 31–43 (1990)
45. A.M. Venezia, G. Pantaleo, A. Longo, G. Di Carlo, M. Casaletto, F.L. Liotta, G. Deganello, J. Phys. Chem. B **109**, 2821–2827 (2005)
46. K.C. Wu, Y.L. Tung, Y.L. Chen, Y.W. Chen, Appl. Catal. B: Environ. **53**, 111–116 (2004)
47. N. Lopez, T.V.W. Janssens, B.S. Clausen, Y. Xu, M. Mavrikakis, T. Bligaard, J.K. Norskov, J. Catal. **223**, 232–235 (2004)
48. S.H. Overbury, L. Ortiz-Soto, H. Zhu, B. Lee, M.D. Amiridis, S. Dai, Catal. Lett. **95**, 99–106 (2004)
49. J.T. Richardson, J.L. Propp, J. Catal. **98**, 457–467 (1986)
50. H.K. Kuo, R.J. De Angelis, J. Catal. **68**, 203–208 (1981)
51. S. Parambadath, A.P. Sing, Catal. Today **141**, 161–167 (2009)
52. M.A. Keane, Appl. Catal. A: Gen. **271**, 109–118 (2004)
53. M.A. Keane, P.M. Patterson, J. Chem. Soc., Faraday Trans. **92**, 1413–1421 (1996)
54. G. Tavoularis, M.A. Keane, J. Chem. Technol. Biotechnol. **74**, 60–70 (1999)
55. M.M. Thackeray, W.I.F. David, J.B. Goodenough, Mater. Res. Bull. **17**, 785–793 (1982)
56. L. Li, C. Jin, X.C. Wang, W.J. Ji, Y. Pan, T. van der Knaap, R. van der Stoel, C.T. Au, Catal. Lett. **129**, 303–311 (2009)
57. B. Klingenberg, M.A. Vannice, Chem. Mater. **8**, 2755–2768 (1996)
58. M. Primeau, C. Vautey, M. Langlet, Thin Solid Films **310**, 47–56 (1997)
59. P. Nkeng, F. Koening, L. Gautier, P. Chartier, G. Poillerat, J. Electroanal. Chem. **402**, 81–89 (1996)
60. S. Wang, B. Zhang, C. Zhao, S. Li, M. Zhang, L. Yan, Appl. Surf. Sci. **257**, 3358–3362 (2011)
61. Y. Brik, M. Kacimi, M. Ziyad, F. Bozon-Verduraz, J. Catal. **202**, 118–128 (2001)
62. B.A. Sexton, A.E. Hughes, T.W. Turney, J. Catal. **97**, 390–406 (1986)
63. M.A. Langell, J.G. Kim, D.L. Pugmire, W. McCarroll, J. Vac. Sci. Technol., A **19**, 1977–1982 (2001)
64. Y. Mikhlin, M. Likhatski, Y. Tomashevich, A. Romanchenko, S. Erenburg, S. Trubina, J. Electron Spectrosc. **177**, 24–29 (2010)
65. L. Makhova, Y. Mikhlin, A. Romanchenko, Nucl. Instrum. Methods A. **575**, 75–77 (2007)
66. J.F. Moulder, W.F. Sticke, P.E. Sobol, K.D. Bomben, in: *Handbook of X-Ray Photoelectron Spectroscopy*, eds. by J. Chastain, R.C. King (Physical Electronics, Eden Prairie, MN, 1995)
67. E.D. Park, J.S. Lee, J. Catal. **186**, 1–11 (1999)
68. M.P. Casaletto, A. Longo, A. Martorana, A. Prestianni, A.M. Venezia, Surf. Interf. Anal. **38**, 215–218 (2006)
69. S. Panigrahi, S. Basu, S. Praharaj, S. Pande, S. Jana, A. Pal, S.K. Gosh, T. Pal, J. Phys. Chem. C **111**, 4596–4605 (2007)
70. X. Zhang, H. Shi, B.Q. Xu, Angew. Chem. Int. Ed. **44**, 7132–7135 (2005)
71. T. Tsoncheva, L. Ivanova, J. Rosenholm, M. Linden, Appl. Catal. B: Environ. **89**, 365–374 (2009)
72. X. Xu, J. Li, Z. Hao, W. Zhao, C. Hu, Mater. Res. Bull. **41**, 406–413 (2006)
73. R.M. Koros, E.J. Nowak, Chem. Eng. Sci. **22**, 470 (1967)